Hindawi
Adsorption Science & Technology
Volume 2023, Article ID 5519783, 19 pages
https://doi.org/10.1155/2023/5519783

Research Article

Development of Efficient Biochar Produced from Orange Peel for Effective La(III) and Y(III) Adsorption

Li Liu,[1] **Bo Feng**,[1,2] **Yun Zhang Rao**,[1,2] **Chang Shun Tian**,[1] **Qi Xiong Gu**,[1] **and Tao Huang**[1]

[1]*Jiangxi Key Laboratory of Mining Engineering, Jiangxi University of Science and Technology, Ganzhou 341000, China*
[2]*School of Resources and Environment Engineering, Jiangxi University of Science and Technology, Ganzhou 341000, China*

Correspondence should be addressed to Bo Feng; 7120220061@mail.jxust.edu.cn

Received 10 April 2023; Revised 19 August 2023; Accepted 9 September 2023; Published 30 September 2023

Academic Editor: Muhammad Iqhrammullah

In this work, orange peel (OP) was used as raw material to produce biochar. The effect of oxygen-limited carbonization temperature (200, 400, and 600°C) on the physicochemical properties and adsorption behavior of orange peel biochar (OPB) toward La(III) and Y(III) in aqueous media was studied. The prepared OPB samples were characterized by SEM, FTIR, and XRD. The experimental results exhibited effective removal of La(III) and Y(III) from aqueous solution by OPB. The carbonization promoted the pore development, and the adsorption process occurred rapidly. The main chemisorption of La(III) and Y(III) on OPB was analyzed by the Langmuir and pseudo-second-order kinetic model, and the participations of electrostatic attraction, exchange, and hydroxyl and carboxyl complexation in OPB were confirmed. The Langmuir maximum capacity of 55.57 mg/g and 31.49 mg/g was obtained at the optimum pH range of 4~6 and the OPB dosage of 1 g/L and 2 g/L for La(III) and Y(III). The efficient orange peel biochar with high adsorption performance can be obtained by considering suitable carbonization temperature.

1. Introduction

Rare earth (RE) is a generic term for the seventeen metal elements in the periodic table, mainly divided into lanthanides, scandium, and yttrium, known as industrial "gold." Because of their excellent physical and chemical properties such as photoelectricity and magnetism, the RE group plays a significant role in military, metallurgy, petrochemical, glass, and ceramics, as well as agriculture and other applications. In recent years, a huge amount of effluent with rare earth elements (REEs) has been generated due to the year-round continuous exploitation and smelting, resulting in serious loss of rare earth resources and pollution of the surrounding environment [1]. Therefore, separation and recovery of REEs in solution have attracted considerable attention. Traditional methods for treating rare earth wastewater mainly include chemical precipitation, ion exchange, solvent extraction, and membrane separation. Most of these methods have their respective advantages in treatment, but there are still shortcomings such as low recovery rate, long separation time, high price, complicated process, secondary pollution, and poor effect of low concentration wastewater treatment [2].

The biochar adsorption technology that has emerged in recent years has shown great potential in the field of heavy metal removal due to its simplicity, low operating cost, high selectivity, fast adsorption and desorption rates, environmentally friendly nature, etc. [3, 4]. Based on the innovative concept of "treating waste with waste," researchers have worked to utilize biological waste to prepare biochar adsorbents and achieved expected recovery results in various metal adsorption applications. Orange peel (OP) has been widely applied due to its low cost and accessibility, mainly focusing on metal-containing [4], organic drugs [5], toxic-oxygenated anions [6], and textile dyes [7]. However, OP as an adsorbent has more restrictions on environmental conditions, and its disadvantages such as weak reactivity, low porosity, and surface area restrict their application in selective and low concentration adsorption [8]. For the reason, several techniques have emerged for the modification of OP,

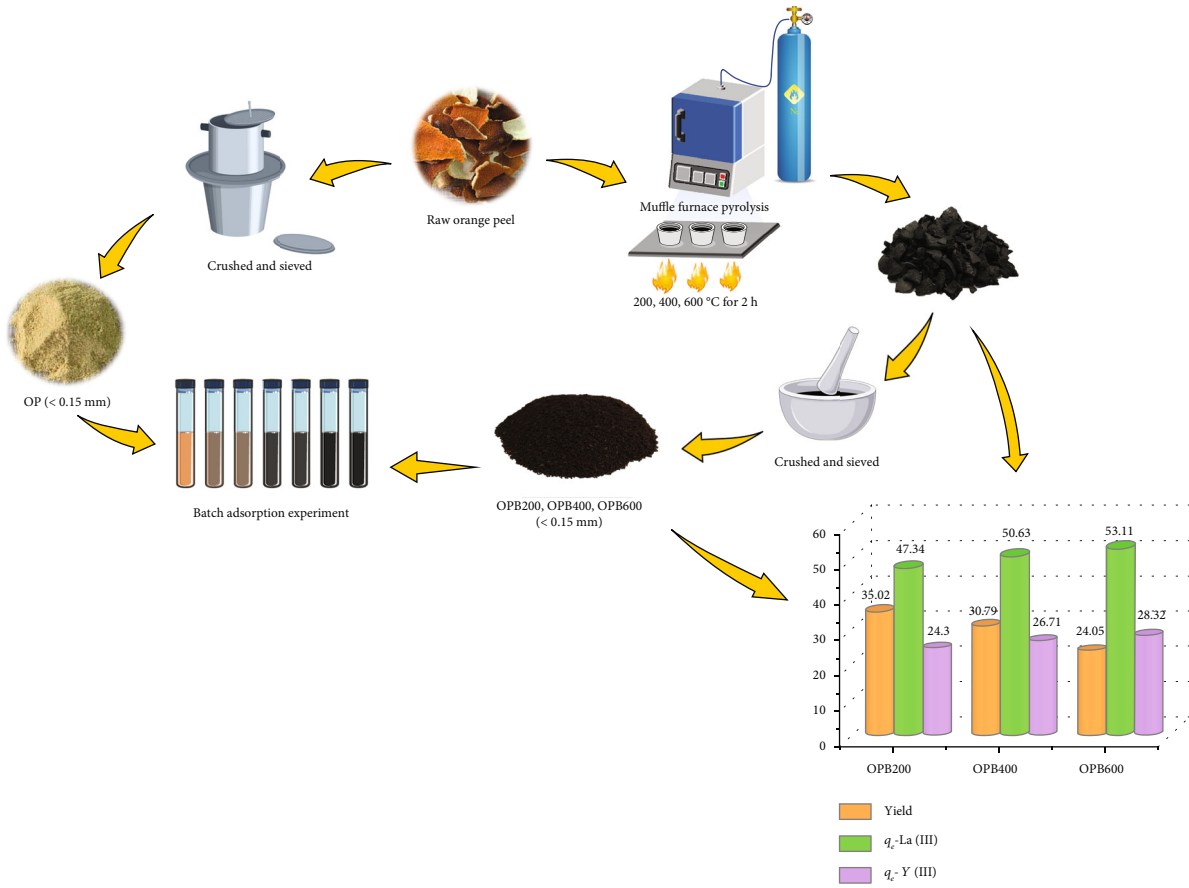

Figure 1: Preparation information of the OPB.

including chemical modification [9], carbonization [10], and activated carbon preparation [11]. Researchers have found that carbonization and thermal activation contribute to improve the stability and adsorption effect of this biomaterial, which is related to its growing specific surface area, abundant mineral content, and pore structure [12–14]. Interestingly, the carbonization temperature at which biochar is prepared plays a crucial role in its quality [15]. Song et al. [15] focused on the effects of biochar composite adsorption performance using different hydrothermal methods (200°C) and pyrolysis temperatures (350°C, 500°C, and 700°C); the optimal temperatures (350°C) and the maximum adsorption (8.163 mg/g) were confirmed. Wu et al. [16] selected spent mushrooms as substrates to carbonize at 300°C, 500°C, and 700°C.

In the literature, the minimum temperature of 200°C was selected for the initial pyrolysis of volatile substance in OP, while the endpoint temperature was 700°C; in general, biochar prepared at charring temperatures above the endpoint temperature contains predominant carbon as the volatile organic compounds have been completely thermally decomposed [17], and these biochars of higher alkalinity and ion exchange capacity within less than 700°C were demonstrated [17, 18]. In order to prevent excessive carbonization of orange peel, a conservative temperature of 600°C was selected in the present work. Therefore, orange peels were exploited to prepare beneficial sorbents by the carbonization at 200, 400, and 600°C; their performance and mechanisms in La(III) and Y(III) adsorption were investigated; and, combined with analysis of SEM, FTIR, and XRD, the physicochemical properties of prepared biochar at three pyrolysis temperatures were compared.

2. Materials and Method

2.1. OPB Preparation. The orange peel (OP) was supplied by local orchards in Ganzhou, China. The supplied OPs were cut into small pieces, washed, and oven-dried to constant weight at 60°C. The dried material was subsequently heated from room temperature to 200, 400, and 600°C (a heating rate of 10°C/min) for 2 h, respectively. This process was conducted under an oxygen-limited condition by using covered corundum crucibles. The resulting biochar was ground and sieved into desirable sizes (less than 0.15 mm) and labeled as OPB. As shown in Figure 1, 35.02%, 30.79%, and 24.05% of OPB200, OPB400, and OPB600 were acquired according to yield formula.

2.2. Characterization Studies. The surface morphology of OPB was observed using an MLA650F-type field emission scanning electron microscope (SEM) (FEI, USA). Infrared spectra before and after adsorption in the wave range of 400-4000 cm^{-1} were recorded by a Nicolet FTIR spectrometer (Vertex 80+Hyperion 2000, China) to obtain the peak changes

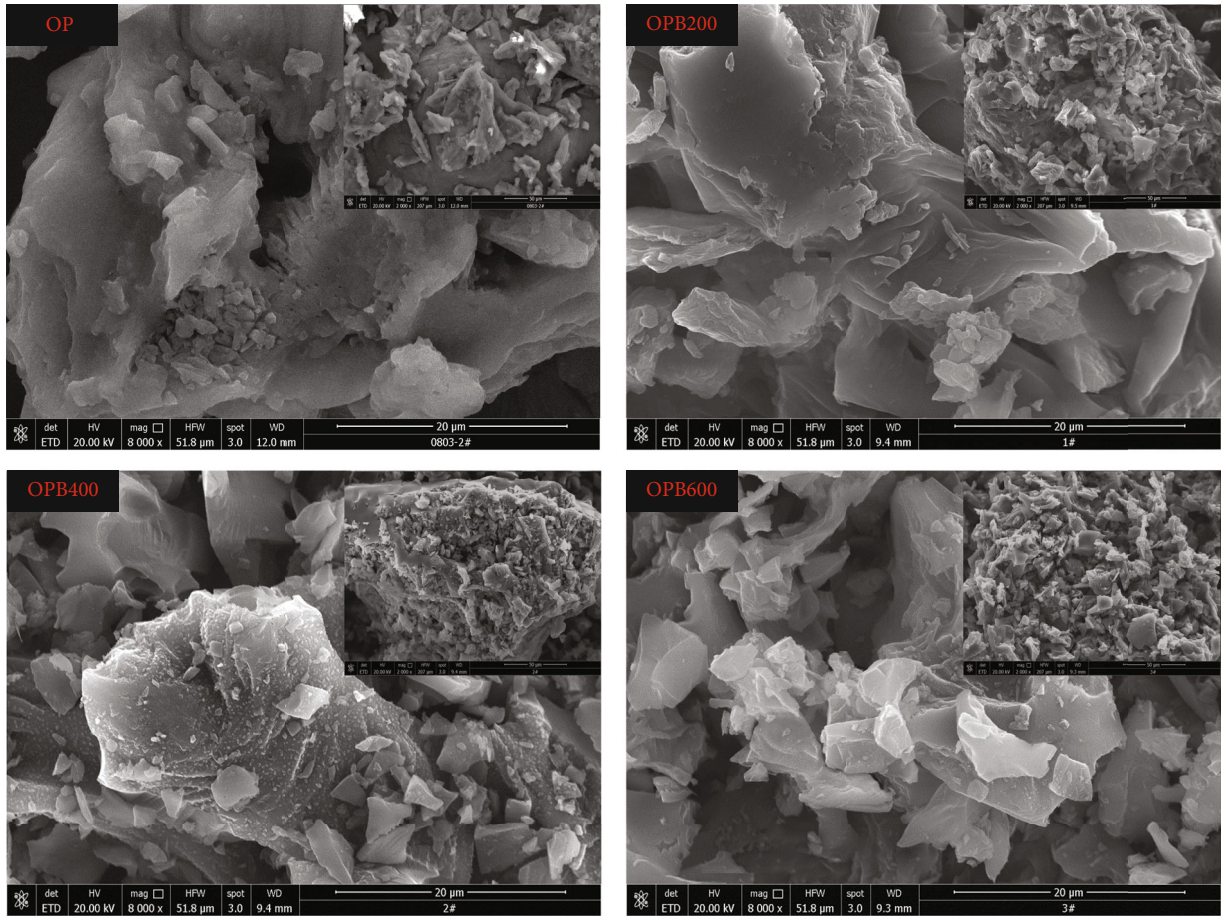

Figure 2: SEM images of OPB at different carbonization temperatures.

of the material functional groups. An X-ray diffractometer (XRD) (Empyrean, The Netherlands) was adopted for the analysis to identify the crystalline phases in the material.

2.3. Adsorption Experiments. The experimental La(III) and Y(III) solutions were prepared by diluting the stock solutions that were produced from $La_2(SO_4)_3$ and $Y_2(SO_4)_3{\cdot}8H_2O$. Batch adsorption experiments were specifically conducted: 50 mL of La(III) and Y(III) solutions with a concentration of 36 mg/L was added to 60 mL test tube bottles, and OPB adsorbent was added at dosage of 1 and 2 g/L, respectively. The mixture was shaken for 2 h at 200 r/min and room temperature. The factor experiments, while remaining other conditions, included the following: (i) the effect of dosage ranged from 0.25 g/L to 5 g/L; (ii) the effect of initial pH ranged from 2 to 7; (iii) adsorption isotherms and thermodynamics at initial La(III) and Y(III) concentration ranged from 5 mg/L to 100 mg/L under temperature of 30, 40, and 50°C; and (iii) adsorption kinetics with contact time ranged from 5 min to 150 min. Three parallel experimental groups were used to calculate the average value. After adsorption, the ion concentration of the supernatant filtered through 0.45 μm filter paper was measured by ultraviolet spectrophotometer (UV-5100).

The adsorption amount (q_e (mg/g)) and the adsorption efficiency (R_e (%)) were calculated as

$$q_e = \frac{(C_0 - C_e) \cdot V}{M},$$
$$R_e = \left(\frac{C_0 - C_e}{C_0}\right) \cdot 100, \quad (1)$$

where C_0 and C_e are the initial and equilibrium concentrations (mg/L), V is the solution volume (L), and M is the mass of OPB (g).

3. Results and Discussion

3.1. Physicochemical Properties. As shown in the SEM image of Figure 2, the surface of OPB was rough and loose and attached with a mass of ash particles. This is because high temperature caused the decomposition of volatile compounds [10, 16]. Due to the adequate carbonation, OPB600 had higher ash content and more surface-attached particles, which increased surface area and available sites for adsorption.

The FTIR analysis of OPB is exhibited in Figure 3. The broad peaks near 3400 cm^{-1} and 2900 cm^{-1} were identified by -OH stretching and -NH bending vibration [9, 19]. The 2731, 2392, 2062, 1759, 824, and 714 cm^{-1} were attributed

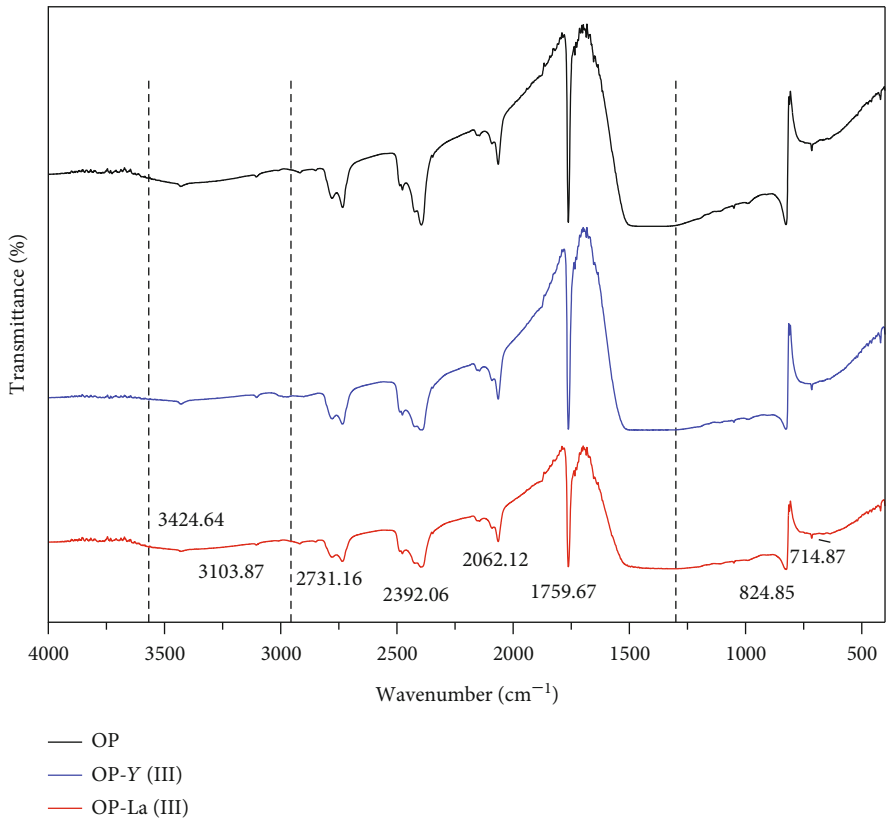

(a) OP [23]

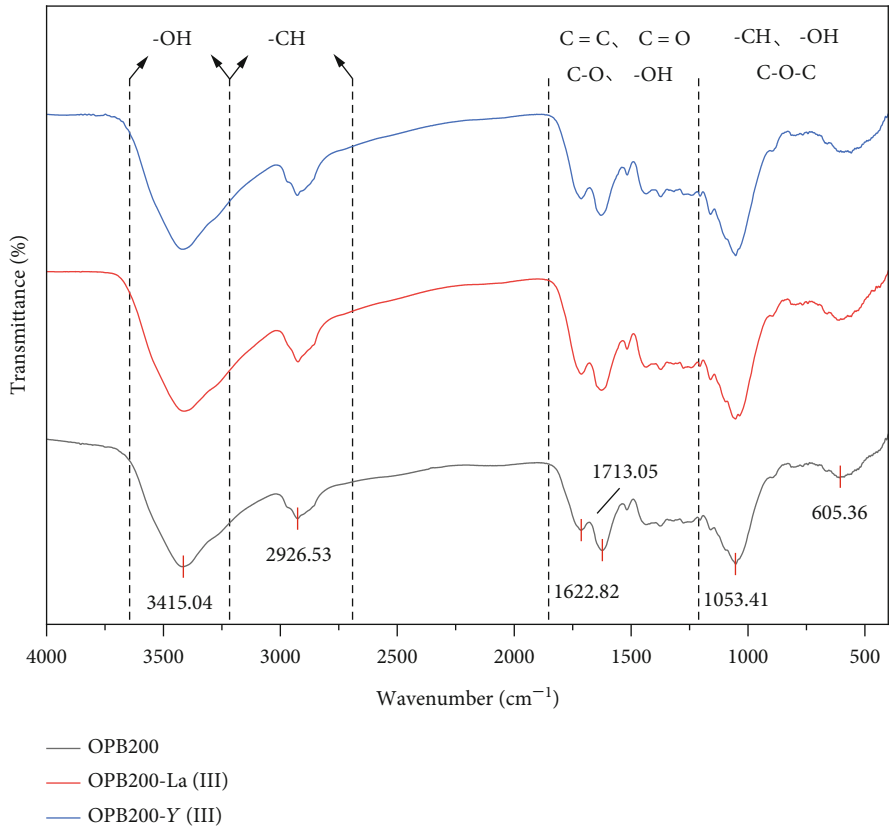

(b) OPB200

Figure 3: Continued.

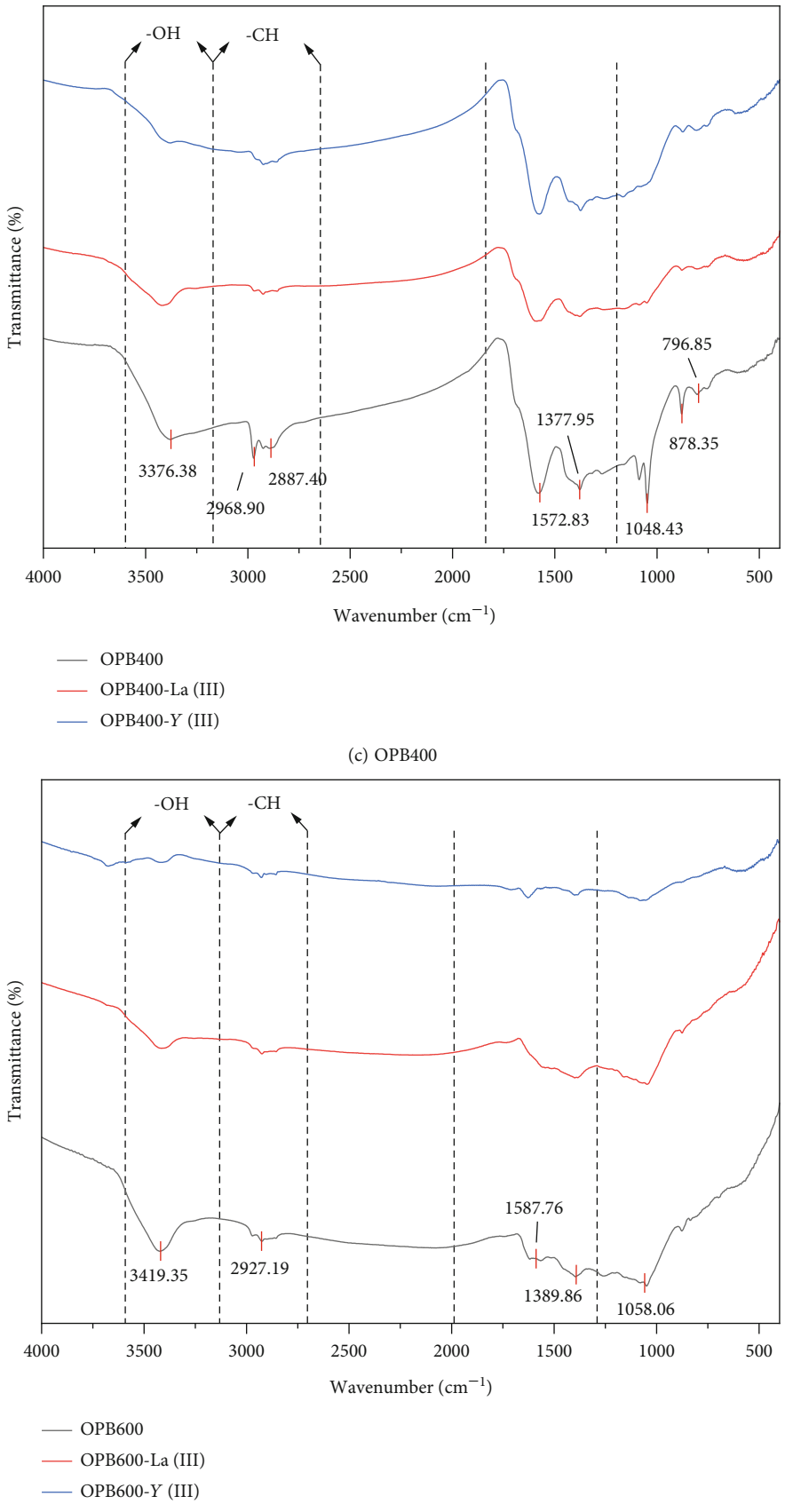

Figure 3: The FTIR spectrum of OPB and OP before and after La(III) and Y(III) adsorption.

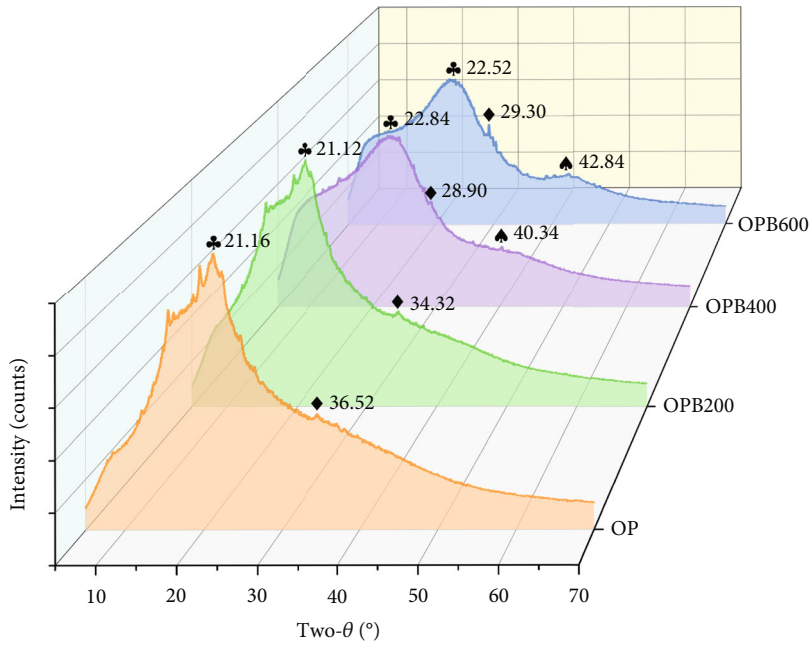

Figure 4: The XRD patterns of OPB and OP.

to vibrations of C=O and C-OH from the alcohol, phenol, ether, and lactone groups in OP, and these oxygen-containing groups (like -OCH_3) are mainly derived from cellulose [20]. The π-electrons provided by these structures could contribute to the adsorption [13, 17]. Similar peaks were displayed in the OPB spectra, but some characteristic peaks near 3400, 2900, 1600, 1300, 1000, and 700cm^{-1} of intensity were weakened or disappeared with higher carbonization temperature. It is noteworthy that for the vibration peak from water molecules, as the preparation temperature increased, the peak of OP shifted from 1759 cm^{-1} to 1587 cm^{-1} of OPB600 and the peak intensity became weaker to inconspicuous. This is due to the decomposition of organic substance and breakdown of chemical bonds by high temperatures, like peaks C=C, C=O, and C-OH; there were fewer acidic functional group on the OPB600 [21, 22]. Therefore, the aromatization was increased in OPB, which is in accordance with most literature that high-temperature biochar has lower O/C, H/C, and (O+N)/C ratios [8].

From the analysis of the XRD pattern of OPB in Figure 4, the small peaks of OP and OPB200 at about $2\theta = 15.50^{\circ}$ suggest that the samples persisted in some imperfect decomposed cellulose structures [16]. The carbon peaks in most region appeared low reflection sharpness, especially OPB400 and OPB600, indicating the noncrystallinity of the structure. Two broad peaks appeared at 20°~25° and 40°~45° were considered to amorphous carbon [14, 24]. This could confirm the presence of some graphite. However, the characteristic peaks of OPB600 at 29.30°~42.84° exhibited greater sharpness and intensity, which were reflections from the mineral components, combined with the FTIR results; this can suggest that higher carbonization temperatures promote organic matter decomposition and mineralization.

3.2. Effect of OPB Dosage. The capacity of adsorbent can be visually expressed through its dosage (S/L). As illustrated in Figure 5, the adsorption efficiency of La(III) and Y(III) increased with increasing OPB dosage, and a maximum was observed at 0.25 g/L to 1 g/L and 2 g/L, respectively. The ions and active sites were sufficiently matched at this optimal dosage; on this premise, the greatest adsorption efficiency of up to 100% could be reached with the appropriate dose of OPB. The adsorption amount decreased as the OPB dosage was incremented. At high biochar dosages, small OPB particles were prone to agglomeration, leading to a decrease in the number of effective adsorption sites, and the tortuous adsorption paths resulting from overlapping particle surface areas can hinder the mass transfer process [25, 26]. In addition, the elevation of solution equilibrium pH value (pH_e) in Figure 6 suggests that the native alkalinity of OPB biochar increased the solution pH, leading to the precipitation of partial RE ions and thus affecting the adsorption [16]. Therefore, surface precipitation contributed to the OPB adsorption.

3.3. Effect of pH. The adsorption trend by OPB at different initial pH is shown in Figure 7. The solution pH often significantly affects the adsorption performance. This is because pH exerts its effect by changing the adsorption system, exactly adsorbate (i.e., RE ions) of species and adsorbent (i.e., biochar) of surface charge in solution [3].

Under the strong acidity conditions, the oxygen-containing functional groups of OPB underwent protonation, resulting in the OPB surface with positive charge. Also, electrostatic repulsion between OPB adsorbents and La(III) and Y(III) occurred due to the undissociated of most of the -COOH or -OH groups, leading to low sorption activity and capacity [3, 17]. In addition, especially low solution pH less than 3.5, the adsorption efficiency of OPB400 and OPB600 was significantly lower than that of OPB200. This means that the herein studied higher temperature biochar was more influenced than lower temperature biochar

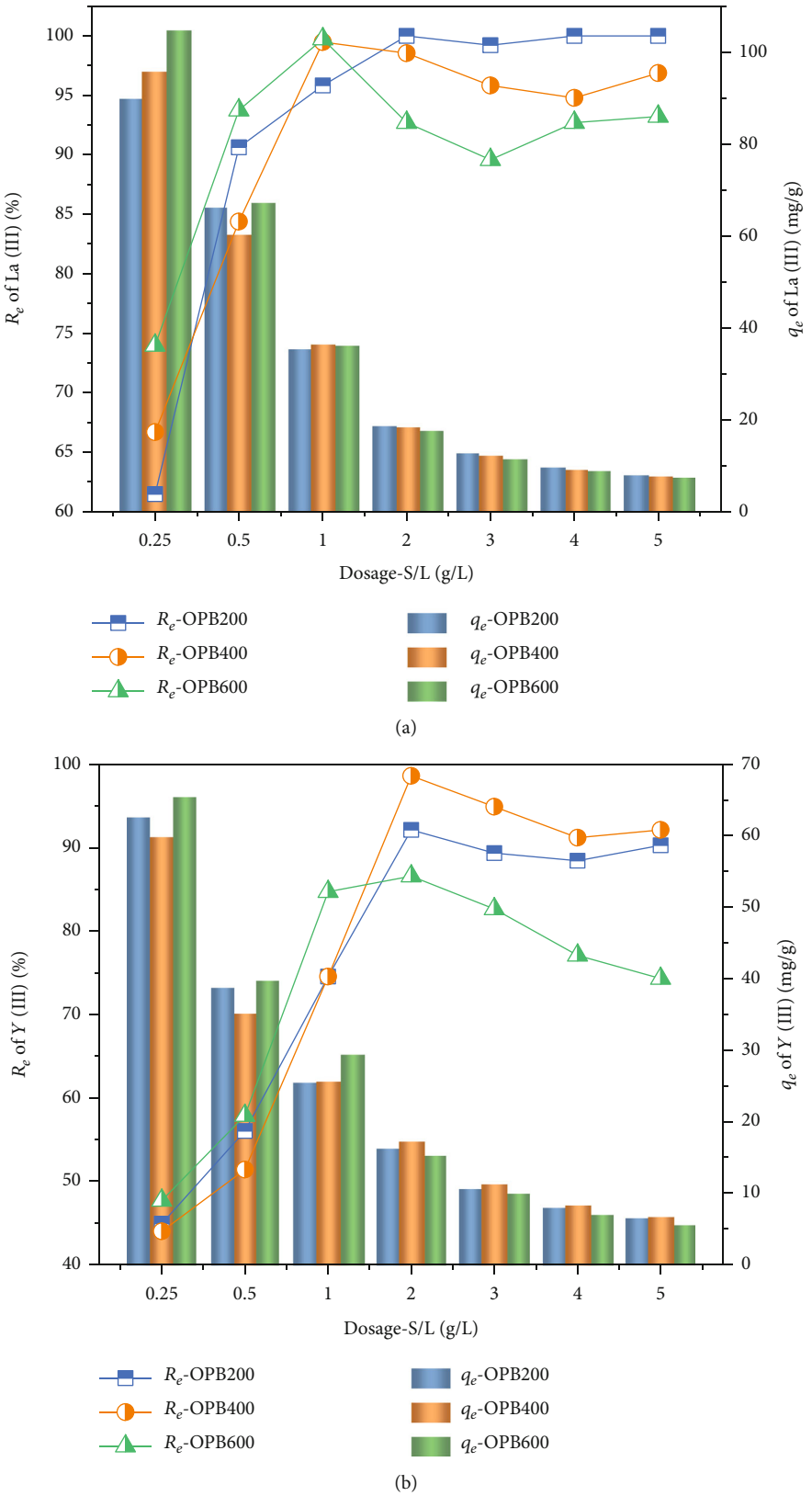

FIGURE 5: Adsorption of La(III) and Y(III) with different OPB dosages (C_0 = 36 mg/L, natural pH (5.11~5.39), t = 2 h, and room temperature (20~25°C)).

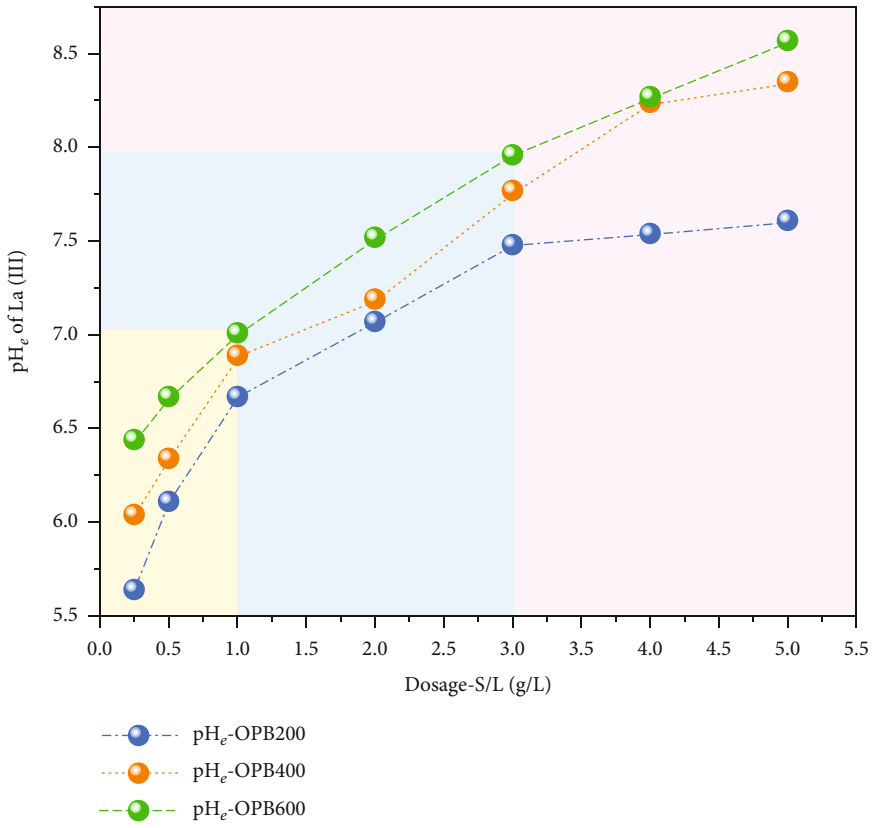

(a)

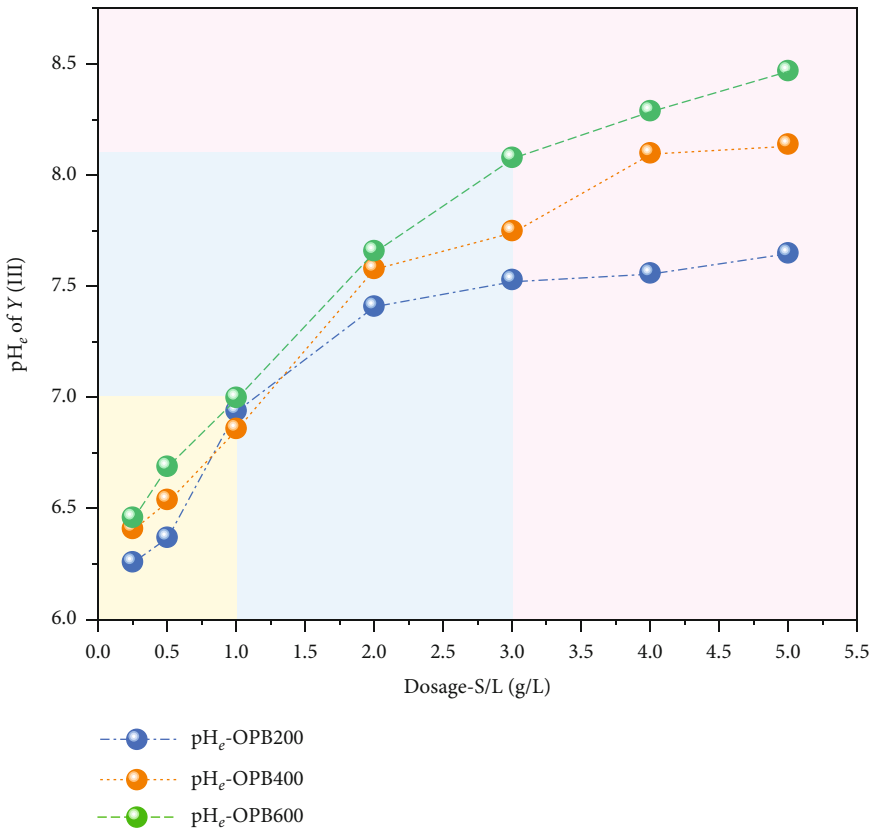

(b)

Figure 6: Equilibrium pH of solution after adsorption.

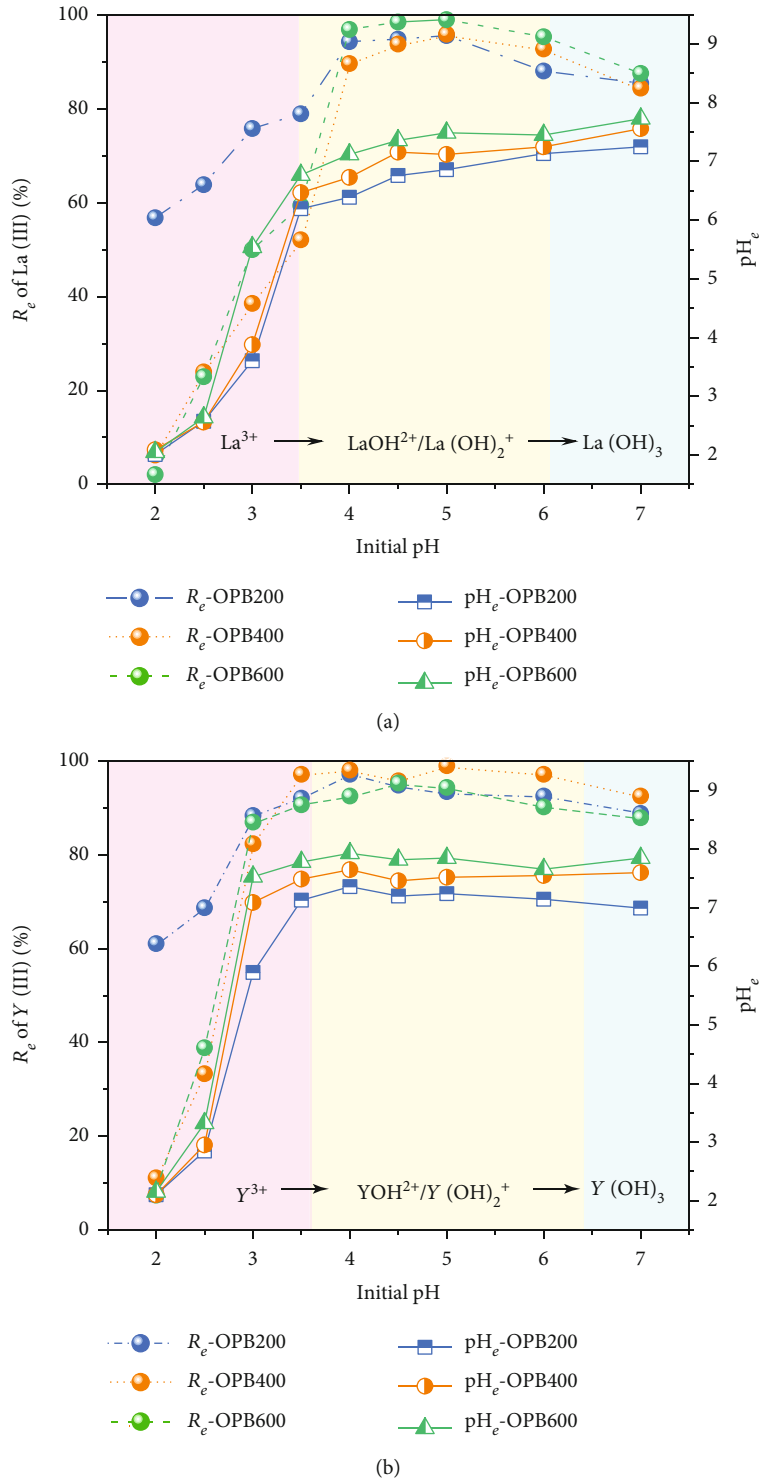

Figure 7: Adsorption for La(III) and Y(III) by OPB with different initial pH (C_0 = 36 mg/L, S/L of La(III) and Y(III) = 1 and 2 g/L, t = 2 h, and room temperature (20~25°C)).

through electrostatic attraction from pH. The elevation of solution pH allowed RE ions to be present in the form of hydroxyl RE ions (e.g., $RE(OH)^{2+}$ and $RE(OH)_2^+$) [27], and the conversion of carboxylic acids into free -COO- forms increased. Therefore, a greater number of RE ions were transferred to the OPB phase via a growing attraction force, which facilitated the interaction of La(III) and Y(III) with the active sites and thus adsorption. Since the smaller effective hydration radius of hydronium ions (H_3O^+ with 0.280 nm) compared to La(III) and Y(III) (~0.452 nm), it is more competitive in occupying the adsorption site on OPB, and the adsorption dominates only when the solution acidity weakens [3, 28].

When the pH values increased from 2.0 to 5.5, the adsorption capacity of OPB adsorbent for La(III) and

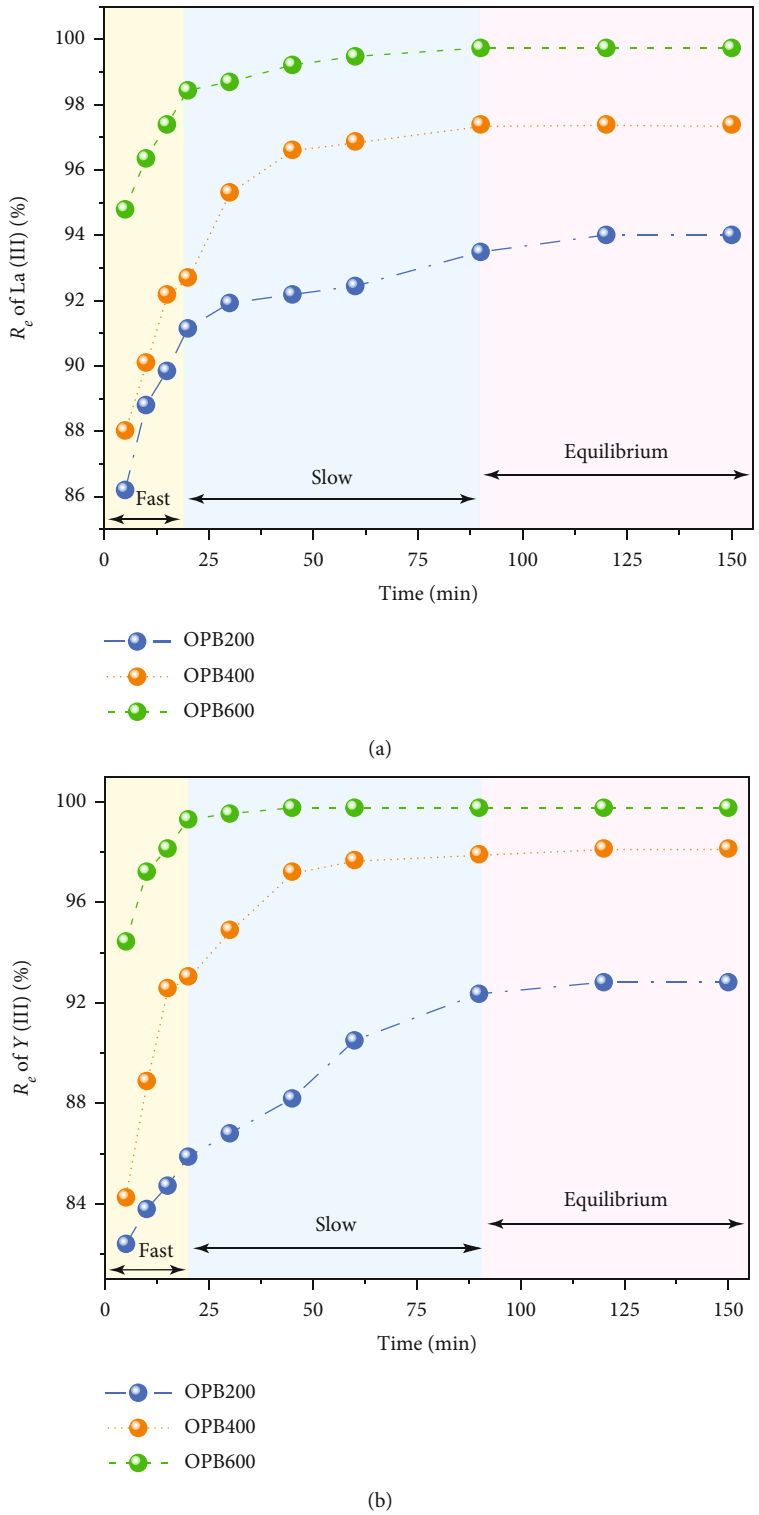

FIGURE 8: La(III) and Y(III) adsorption by OPB with contact time (C_0 = 36 mg/L, S/L of La(III) and Y(III) = 1 and 2 g/L, natural pH (5.11~5.39), and room temperature (20~25°C)).

Y(III) has increased and reached its maximum. Clearly, this result suggests that electrostatic attraction was an existence of dominating contribution in the adsorption process (namely, pore filling and physical adsorption as secondary contributions). With rising pH above 6, the pH_e values remained around 7 or 8; in this state, a portion of RE ions precipitated as hydroxide ($RE(OH)_3$), which is the main factor for the diminished extent of OPB adsorption, consequently reducing the adsorption efficiency [3].

3.4. Effect of Contact Time. As shown in Figure 8, the overall adsorption was a process of first fast and then slow and finally reaches equilibrium, which indicates the effective role of surface sites and porous structure of the carbonaceous adsorbent. Initially, the fast adsorption stage completed within about 25 min, and the La(III) and Y(III) adsorption by OPB600 reached more than 98%. It is noteworthy that this stage with relatively faster adsorption process was attributed to the abundance of vacant binding sites and the higher gradient concentration between solute and adsorbent phases, which prompted a greater accessibility of La(III) and Y(III) to active sites in the OPB surface [25].

Then, the slow adsorption phase proceeded because of the almost saturation in OPB surface sites. At this point, prolongation of equilibrium time resulted from diffusion of residual ions and obstruction of mass transfer processes [4], OPB200 adsorption duration within 60 min, while a much shorter time, about 30 min, was required for OPB600 and achieved a higher adsorption efficiency. This is mainly because the increased pore structure of OPB600 after carbonization at high temperature was conducive to the adsorption process. In the final stage, the adsorption efficiency did not vary with time, implying the equilibrium relationship between the desorption and adsorption.

3.5. Effect of Initial La(III) and Y(III) Concentration. As can be seen in Figure 9, the adsorption efficiency for La(III) and Y(III) decreased almost linearly upon the increase of the initial concentration from 5 to 100 mg/L. At lower initial concentrations, the optimum adsorption amount was 66.03 mg/g for La(III) and 35.14 mg/g for Y(III). This is because of the driving force provided by the gradient difference between the low concentration ions and the high mass adsorbent, which promotes the approach of ions to adsorbents [25], which can also be considered as a strong adsorption force generated from the unsaturated sites of OPB and targeted to the low concentration of RE ions. However, a fixed amount of OPB has a limited maximal adsorption capacity. As a result, as the initial concentration increases, the adsorption efficiency of the RE ions was negatively affected, mainly because the saturation of available adsorption sites would limit the interaction between RE ions and OPB. Consequently, the optimum adsorption depends on the ratio of adsorbent dosage to ion concentration.

On the other hand, OPB600 kept the highest equilibrium adsorption capacity, followed by OPB400. Similar results were obtained on wood ear mushroom stick-derived biochar [26] and microalgal residue-derived biochar [29], for adsorption of Cd(II) and Pb(II). These observations disclosed that biochar prepared at higher temperatures has an available surface structure for adsorption and greater adsorption affinity for ions, resulting in better adsorption capacity.

4. Adsorption Model

4.1. Kinetic Studies. This study adopted the pseudo-first-order kinetic (PFO) (Equation (2)), pseudo-second-order kinetic (PSO) (Equation (3)), and Weber-Morris model (intraparticle diffusion model) (Equation (5)) to analyze the experimental results.

$$\log (q_e - q_t) = \log q_e - \frac{K_1 t}{2.303}, \tag{2}$$

where q_t is the adsorption amount at time t (mg/g) and K_1 is the PFO constant (1/min).

$$\frac{t}{q_t} = \frac{1}{K_2 q_e^2} + \frac{t}{q_e}, \tag{3}$$

where K_2 is the PSO constant (g/(mg·min)) and K_2 can calculate H, the initial adsorption rate constant (mg/(g·min)), indicating the rapidity for attaining an equilibrium state, according to the following:

$$H = K_2 q_e^2. \tag{4}$$

As illustrated in Table 1, the OPB adsorption for La(III) and Y(III) with higher fit coefficient R^2 obeyed the PSO kinetics, and the experimental result $q_e(\exp)$ coincided with theoretical value $q_e(\text{cal})$. This implies that chemisorption dominated the main rate-limiting step in the OPB adsorption [30]. The K_2, q_e, and H values of OPB600 were larger than OPB400 and OPB200, indicating the higher adsorption capacity and shorter equilibrium adsorption time of prepared OPB at higher carbonization temperature. One of the explanations is the pore development of the carbonization process [10].

$$q_t = K_p t^{1/2} + C, \tag{5}$$

where K_p is the intraparticle diffusion rate constant (m·g/(gmin$^{1/2}$)) and C relate to the boundary layer thickness.

The graph plotted from q_t versus $t^{1/2}$ (Figure 10) was divided into two kinetic adsorption phases. The diffusion rate in the first stage was higher than that in the second stage. The OPB surface was well adsorbed with La(III) and Y(III) due to the greater external mass transfer process [31]. These lines without passing through the origin indicate that the adsorption rate depended on intraparticle diffusion and were controlled by multiple steps together [4, 32]. The increase in boundary layer thickness may affect the progression of equilibrium adsorption. Therefore, the value C_1 was less than C_2, which further confirmed the intimate correlations between particle internal diffusion and surface reaction, external diffusion, and liquid film diffusion [33].

4.2. Adsorption Isotherm Studies. The interaction between adsorbent and adsorbate can be elucidated by isothermal adsorption. Three classical isothermal adsorption models, Langmuir (Equations (6) and (7)), Freundlich (Equation (8)), and Dubinin-Radushkevich (D-R) (Equations (9)–(11)), were employed to calculate the model fitting parameters, and the results are presented in Tables 2 and 3.

$$\frac{C_e}{q_e} = \frac{C_e}{q_{max}} + \frac{1}{q_{max} K_L}, \tag{6}$$

where q_{max} stands for the maximal monolayer adsorption capacity (mg/g) and K_L represents the equilibrium constant

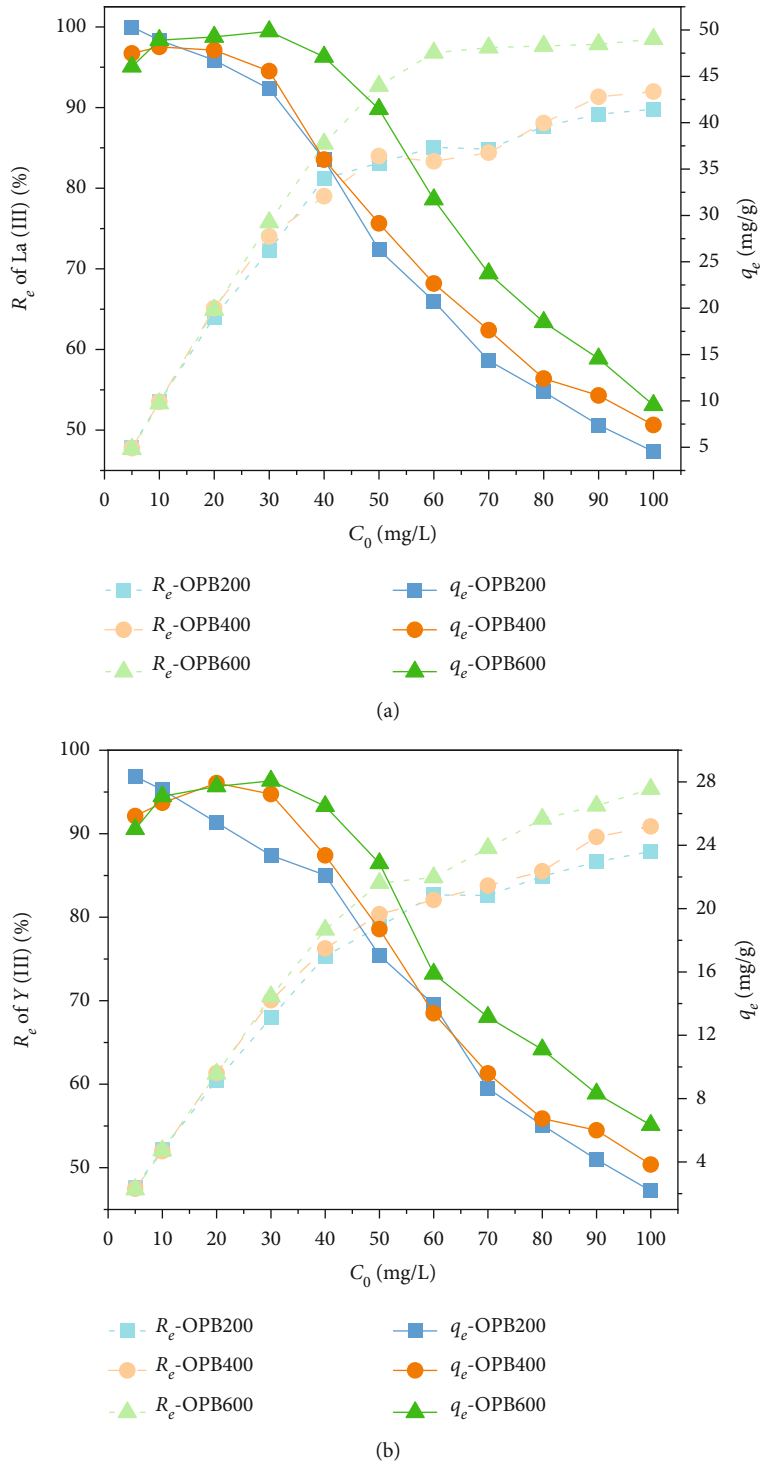

Figure 9: La(III) and Y(III) adsorption by OPB with different initial concentrations (S/L of La(III) and Y(III) = 1 and 2 g/L, t = 2 h, natural pH (5.11~5.39), and room temperature (20~25°C)).

related to the apparent energy of adsorption (L/mg), which signifies the adsorption capacity. Both values can be afforded by plotting C_e/q_e against C_e. The essential feature of the Langmuir model can be evaluated by equilibrium parameter R_L [20].

$$R_L = \frac{1}{1 + K_L C_0}. \quad (7)$$

If $0 < R_L < 1$, adsorption is favorable, $R_L > 1$ unfavorable, and $R_L = 0$ irreversible process [34].

$$\log q_e = \log K_F + \frac{1}{n} \log C_e, \quad (8)$$

Table 1: Kinetic model parameters of OPB adsorption.

Model	Parameter	La(III)			Y(III)		
		OPB200	OPB400	OPB600	OPB200	OPB400	OPB600
	q_e(exp)	34.09	35.31	36.16	16.10	17.02	17.31
PFO	K_1	0.03	0.06	0.05	0.04	0.05	0.14
	q_e	2.36	4.47	1.88	2.59	2.50	2.57
	R^2	0.922	0.979	0.965	0.937	0.940	0.836
PSO	K_2	0.03	0.04	0.08	0.04	0.05	0.20
	q_e	34.24	35.55	36.26	16.28	17.17	17.35
	H	43.42	43.44	105.71	9.26	15.09	58.69
	R^2	0.999	0.999	1	0.999	0.999	0.999

where K_F (L/mg) and n denote the Freundlich constants, which are associated with the adsorption capacity and intensity.

From the table results, the adsorption for La(III) and Y(III) on OPB in this solution concentration range conformed better to the Langmuir model. It can be concluded that the adsorption has proceeded via a monolayer covering homogenous process [35, 36]. The R_L values of La(III) and Y(III) in the range between 0 and 1 represent the satisfied condition for favorable adsorption on OPB. Notably, OPB200 adsorption may occur multilayer chemisorption, as indicated by its higher coefficient R^2 for the Freundlich model, which reveals that the increase of preparation temperature caused the biochar to tend to the incremental adsorption of monolayer.

The $1/n$ values < 0.4, suggesting a heterogeneous surface of OPB and its great adsorption characteristics [5, 9]. Also, the higher values of q_{max} and n in higher temperature environment are indicative of the better adsorption performance in a certain range. The rule that the K_L, R_L, and K_F values of La(III) calculated were higher than those of Y(III) is consistent with their ionic radius; that is, the smaller the radius of the hydrated ions, the higher the affinity and adsorption strength for OPB.

The D-R model can be applied to estimate the apparent free energy and determine the role of microporous adsorption [37]. The formulas are as follows:

$$\ln q_e = \ln Q_m - K_D \varepsilon^2, \tag{9}$$

where Q_m (mg/g) is the saturation adsorption amount and ε denotes the Polanyi potential (J/mol) and has the following form:

$$\varepsilon = RT \ln\left(1 + \frac{1}{C_e}\right). \tag{10}$$

R is the universal gas constant (8.314 J/(mol·K)), and T is the absolute temperature. Generally, K_D (mol^2/kJ^2) is a D-R constant with energy dimension, which can obtain the E_s (kJ/mol), the average free energy of adsorption.

$$E_s = \frac{1}{\sqrt{2K_D}}. \tag{11}$$

From the results, the less E_s values of OPB600 than OPB400 and followed by OPB200, which disclosed that the physical action of OPB adsorption, were enhanced via carbonization modification. Since the E_s magnitude for a physical adsorption process ranges from 1 to 8 kJ/mol and a chemical adsorption process ranges from 8 to 16 kJ/mol, the E_s values are around 8 kJ/mol with a rise in solution temperature, indicating that the adsorption process proceeded with physical-chemical cointeraction.

4.3. Thermodynamic Studies. The adsorption properties and thermodynamic behavior of OPB on La(III) and Y(III) can be predicted by the Gibbs parameter analysis. The relevant equations are as follows:

$$\begin{aligned} K_d &= K_L \times C_0 \times 10^3, \\ \ln K_d &= -\frac{\triangle G^\theta}{RT} = \frac{\triangle S^\theta}{R} - \frac{\triangle H^\theta}{RT}, \\ \triangle G^\theta &= -RT \ln K_d, \end{aligned} \tag{12}$$

where K_d is the equilibrium constant. The value of ΔG^θ, ΔH^θ, and ΔS^θ can be calculated from the slope and intercept by plotting the Van't Hoff graph.

Table 4 shows the calculation results of thermodynamic parameters. The adsorption behavior of La(III) and Y(III) on OPB can be inferred as a spontaneous reaction from negative ΔG^θ values. Furthermore, the increased $|\Delta G^\theta|$ with increased temperature indicate that the adsorption process is essentially an endothermic reaction, which is also evidenced by the positive ΔH^θ values, and hence is more likely to be carried out at higher temperatures. As mentioned in the literature, the ΔH^θ values at 20~400 kJ/mol indicates that chemisorption mechanism plays a major role [29]. In this study, the ΔH^θ for La(III) and Y(III) ranged at 20.97~25.56 kJ/mol suggest that the adsorption on OPB was of chemisorption type, and the processes proceeded through electrostatic interactions and chelation from functional portions of the adsorbent surface. Besides, the positive values of ΔS^θ suggest that the adsorption system was driven

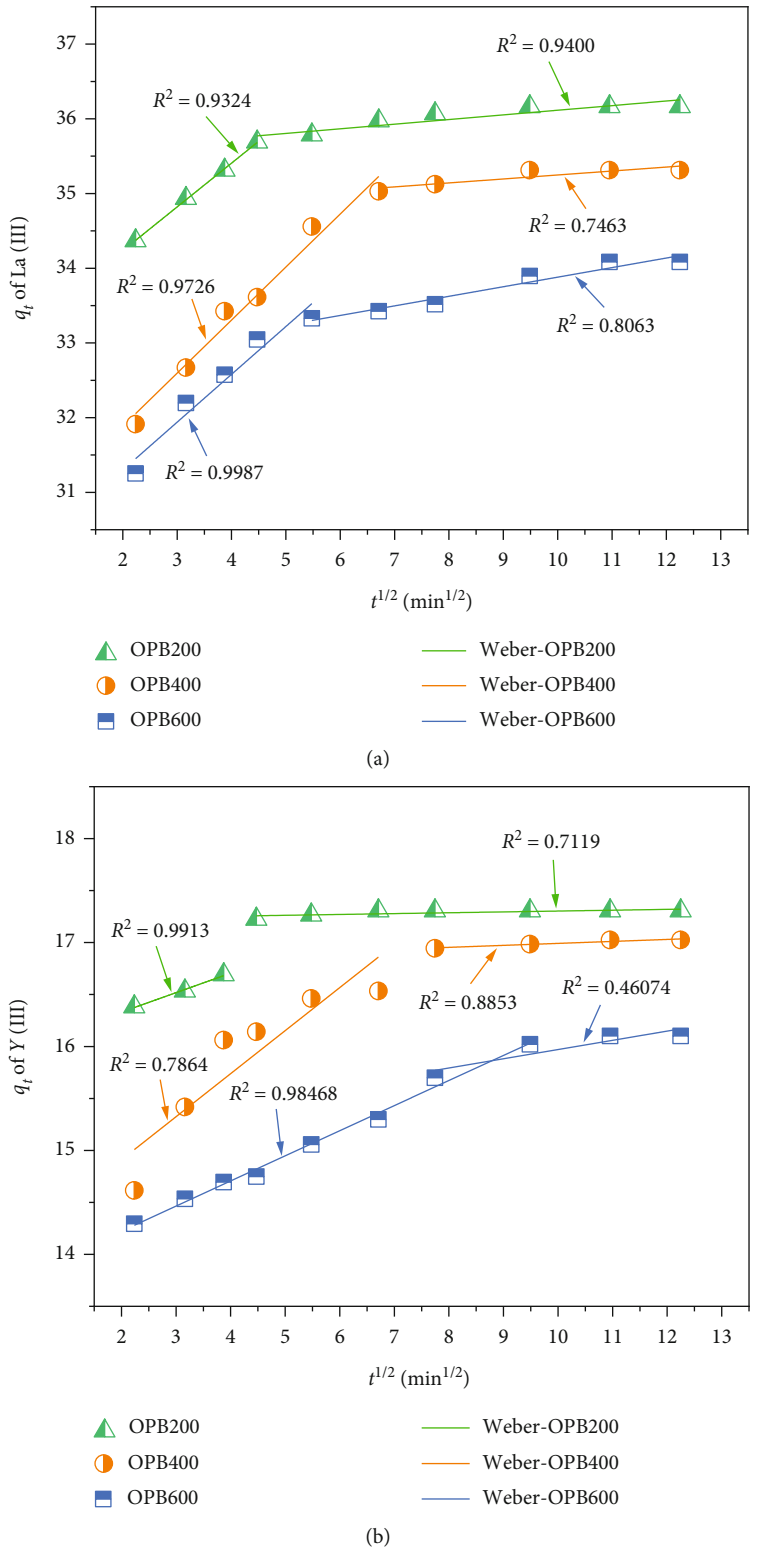

Figure 10: Linear fitting of the Weber model for La(III) (a) and Y(III) (b).

by an increase in entropy, which means that during the adsorption process, the randomness of the solid-liquid interface increased [38], which is considered to have more ion exchanges [7].

4.4. Adsorption Mechanism. Table 5 compares the adsorption capacity of La(III) and Y(III) between the prepared biochar and other biochar reported in the literature. The orange peel-derived biochar displays higher adsorption capacities

Table 2: Isotherm parameters of La(III) adsorption on OPB.

Model	Parameter	OPB200 (K)			OPB400 (K)			OPB600 (K)		
		293	303	313	293	303	313	293	303	313
	q_m(exp)	41.46	47.34	51.85	43.35	50.63	52.79	49.01	53.10	55.57
Langmuir	q_{max}	46.93	46.93	47.42	49.63	50.40	50.56	53.82	53.71	54.62
	K_L	0.46	0.51	0.40	0.45	0.43	0.42	0.80	0.90	0.65
	R_L (5~100 mg/L)	0.02~0.30	0.02~0.28	0.03~0.33	0.02~0.30	0.02~0.32	0.02~0.33	0.01~0.20	0.01~0.18	0.02~0.24
	R^2	0.992	0.992	0.990	0.988	0.991	0.991	0.999	0.997	0.996
Freundlich	K_F	18.90	18.65	15.26	19.28	15.73	15.53	17.62	24.00	16.97
	$1/n$	0.24	0.25	0.31	0.31	0.33	0.34	0.31	0.27	0.31
	R^2	0.978	0.948	0.933	0.915	0.856	0.867	0.690	0.573	0.541
D-R	K_D	3.87	5.83	5.24	6.00	8.87	9.51	11.66	5.76	18.07
	Q_m	38.92	37.40	37.17	40.76	40.70	40.35	48.57	46.01	51.86
	E_s	11.37	9.26	9.77	9.13	7.51	7.25	7.63	9.31	5.26
	R^2	0.871	0.792	0.917	0.937	0.956	0.938	0.992	0.523	0.975

Table 3: Isotherm parameters of Y(III) adsorption on OPB.

Model	Parameter	OPB200 (K)			OPB400 (K)			OPB600 (K)		
		293	303	313	293	303	313	293	303	313
	q_m(exp)	23.61	24.30	27.16	25.19	26.71	28.34	27.55	28.32	31.49
Langmuir	q_{max}	24.11	23.97	21.51	29.13	26.84	26.32	29.47	28.60	23.28
	K_L	0.20	0.21	0.22	0.16	0.17	0.18	0.17	0.17	0.20
	R_L (5~100 mg/L)	0.33~0.90	0.33~0.91	0.31~0.90	0.38~0.93	0.36~0.92	0.36~0.92	0.37~0.92	0.37~0.92	0.33~0.91
	R^2	0.990	0.995	0.979	0.979	0.987	0.970	0.969	0.996	0.968
Freundlich	K_F	6.65	9.08	10.27	6.97	7.61	8.48	7.78	8.86	11.30
	$1/n$	0.37	0.27	0.24	0.38	0.36	0.34	0.40	0.38	0.34
	R^2	0.932	0.955	0.963	0.791	0.892	0.822	0.713	0.688	0.646
D-R	K_D	9.26	5.60	3.13	24.17	9.35	8.70	29.19	17.99	7.37
	Q_m	17.88	18.72	21.02	21.98	20.38	21.22	26.05	25.63	26.75
	E_s	7.35	9.44	12.63	4.55	7.31	9.58	4.14	6.27	8.23
	R^2	0.798	0.712	0.9537	0.959	0.918	0.944	0.982	0.942	0.923

Table 4: Thermodynamic model parameters of La(III) and Y(III) adsorption by OPB.

Type	Samples	ΔG^θ (kJ/mol)			ΔH^θ (kJ/mol)	ΔS^θ (J/mol·K)
		293 K	303 K	313 K		
La(III)	OPB200	-24.48	-25.56	-25.76	22.69	168.73
	OPB400	-24.42	-25.11	-25.87	23.39	172.66
	OPB600	-25.82	-27.00	-27.02	25.56	178.20
Y(III)	OPB200	-21.92	-22.89	-23.65	20.97	149.65
	OPB400	-22.02	-22.79	-24.00	22.52	151.40
	OPB600	-22.45	-23.21	-24.20	23.67	154.64

Table 5: Comparison of the adsorption capacity of orange peel carbon and other biochar-modified materials for La(III) and Y(III) (adsorption temperature: 22°C~25°C).

Adsorbents	Metals	Concentration (mg/L)	Dosage (g/L)	q_m (mg/g)	References
OPB (200~600°C)	La(III)	36	1	41.46~49.01	This study
	Y(III)	36	2	23.61~27.55	
Sargassum fusiforme AC (300~700°C)	La(III)	25~500	1	170.36~275.48	[39]
Biochar composites	Lanthanides	50~200	5	11.10	[40]
Rice husk AC (500°C)	La(III)	150	10	14.46	[41]
	Y(III)	150	10	13.42	
AC	La(III)	10~200	40	94.46	[42]
Bamboo charcoal	La(III)	135~270	0.67	120	[43]
Pectin (banana peel) AC	La(III)	Leachate	—	21.80	[44]
	Y(III)	Leachate	—	27.78	
Banana peel AC	Lanthanides	100	2	470.11(I)	[45]

Note: AC: activated carbon. Lanthanides are the measured value of La(III) in lanthanide solution.

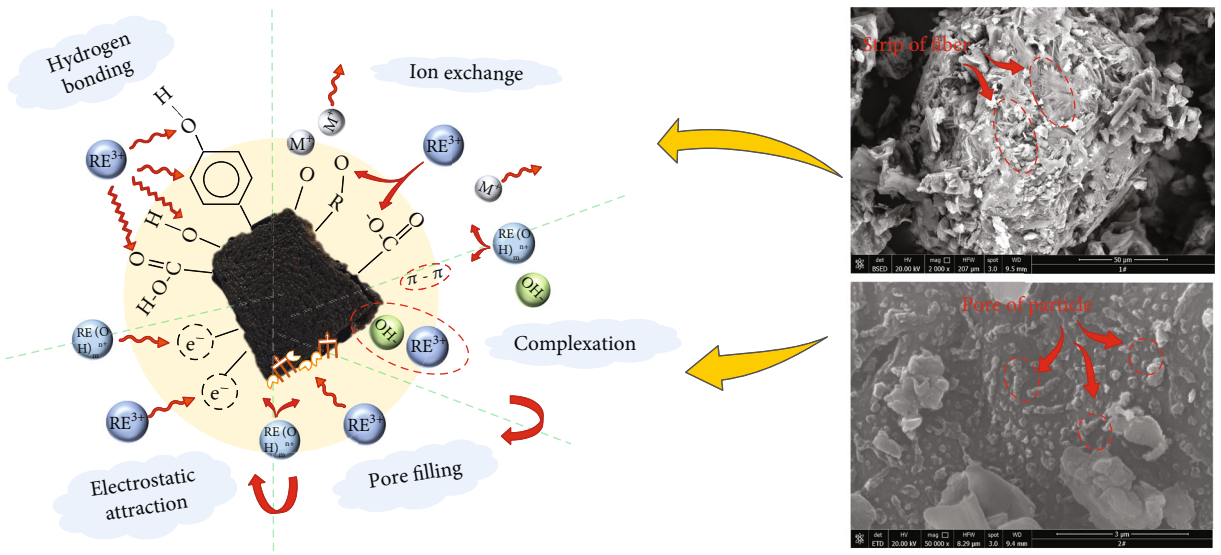

Figure 11: Adsorption mechanism of La(III) and Y(III) on OPB.

than some other biochar. The result affirms that OPB could be recruited as valuable adsorbents with high adsorption capacities for recycle of rare earth ions from water medium.

Due to the plentiful nature of biomass and biochar, their adsorption mechanism for RE ions is relatively complex. The FTIR spectra in Figure 3 show various oxygen-containing functional groups on OPB. These active groups adsorbed RE ions in solution though hydrogen bonding and also π-π interaction as a primary adsorption mechanism owing to the high aromaticity structure of OPB, which can be found from the shift of peak positions and the decrease of the peak intensity [9, 13, 46]. Physisorption is critical for the adsorption of carbon-based adsorbent materials. OPB is a carbonaceous material with well-developed porous, and this porosity property can utilize a pore filling mechanism to improve the adsorption capacity for La(III) and Y(III), especially at high-temperature adsorption [17]. The adsorbent dosage affected the equilibrium pH_e value of the solution and thus affected the adsorption process along with the initial pH. Previous literatures have mentioned that the alkalinity of inorganic minerals in biochar would participate in the precipitation process of ions [15]. In addition, the impact of pH determined the coexistence of electrostatic interaction and coupling effect in the adsorption process. Based on the HSAB theory (Hard-Soft-Acid-Base), the functional groups of adsorbents and RE ions can act as the Lewis acid-base, and this phenomenon plays a basic role in the surface complexation on OPB [47]. According to the study of Kołodyńska et al. [40], the equation was proposed:

$$\mathrm{ROOH} + \mathrm{Re}\,(\mathrm{OH})_n^{m+} \longrightarrow \mathrm{ROORe(OH)}_n + m\mathrm{H}^+. \quad (13)$$

Taken together, as illustrated in Figure 11, OPB with higher preparation temperatures, the main contributions in

adsorption process were electrostatic attraction and pore filling, as well as functional group action, hydrogen bond formation, and ion exchange [17, 48]. The isothermal, kinetic, and thermodynamic analyses concluded that the driving force of La(III) and Y(III) in solution enhanced at higher ion concentrations and higher temperatures, which accelerated their diffusion and purposeful approach to the OPB adsorbents, thereby promoting the feasibility and spontaneity of adsorption.

5. Conclusions

This study demonstrates the properties of orange peel-derived biochar prepared at three carbonization temperatures, and the prepared samples were used as adsorbents to study the adsorptive behavior of La(III) and Y(III). The prepared OPB exhibited well-developed porosity characters and were influenced by the carbonization temperature. OPB are carbonaceous mesoporous adsorbents with abundant surface sites and functional groups, which facilitated the coordination with ions. The OPB600 exhibited better adsorption capacity, and the Langmuir adsorption amounts of La(III) and Y(III) reached 55.57 mg/g and 31.49 mg/g. This study confirms that orange peel biochar, as a cost-effective adsorbent, can be applied to the treatment of La(III)- and Y(III)-contaminated water.

Data Availability

All relevant data during this study are included within the article.

Conflicts of Interest

The authors declare no competing interest.

Authors' Contributions

Li Liu conceptualized the study and prepared the first draft of the manuscript. Bo Feng, Tao Huang, and Qi Xiong Gu supervised the study and wrote, reviewed, and edited the manuscript. Chang Shun Tian and Yun Zhang Rao were responsible for funding acquisition.

Acknowledgments

The authors acknowledge the financial support from the National Natural Science Foundation of China (51964014) and Program of Science and Technology Research, Education Department of Jiangxi Province (GJJ200814).

References

[1] Q. X. Gu, Z. Huang, S. J. Li, W. Zeng, and K. Zhao, "An approach for water-inrush risk assessment of deep coal seam mining: a case study in Xinlongzhuang coal mine," *Environmental Science and Pollution Research*, vol. 27, no. 34, pp. 43163–43176, 2020.

[2] Y. R. Lee, K. Yu, S. Ravi, and W. S. Ahn, "Selective adsorption of rare earth elements over functionalized Cr-MIL-101," *ACS Applied Materials and Interfaces*, vol. 10, no. 28, pp. 23918–23927, 2018.

[3] A. Rahmani-Sani, P. Singh, P. Raizada et al., "Use of chicken feather and eggshell to synthesize a novel magnetized activated carbon for sorption of heavy metal ions," *Bioresource Technology*, vol. 297, article 122452, 2020.

[4] A. E. Nemr, R. M. Aboughaly, A. E. Sikaily, S. Ragab, M. S. Masoud, and M. S. Ramadan, "Microporous nano-activated carbon type I derived from orange peel and its application for Cr(VI) removal from aquatic environment," *Biomass Conversion and Biorefinery*, vol. 12, no. 11, pp. 5125–5143, 2022.

[5] A. Pandiarajan, R. Kamaraj, S. Vasudevan, and S. Vasudevan, "OPAC (orange peel activated carbon) derived from waste orange peel for the adsorption of chlorophenoxyacetic acid herbicides from water: adsorption isotherm, kinetic modelling and thermodynamic studies," *Bioresource Technology*, vol. 261, pp. 329–341, 2018.

[6] B. P. Mora, F. A. Bertoni, M. F. Mangiameli, J. C. González, and S. E. Bellú, "Batch and fixed-bed column studies of selenite removal from contaminated water by orange peel-based sorbent," *Water Science and Engineering*, vol. 13, no. 4, pp. 307–316, 2020.

[7] A. Daouda, A. T. Honorine, N. G. Bertrand, D. Richard, and D. Domga, "Adsorption of rhodamine B onto orange peel powder," *American Journal of Chemistry*, vol. 9, pp. 142–149, 2019.

[8] M. Salman, M. Athar, and U. Farooq, "Biosorption of heavy metals from aqueous solutions using indigenous and modified lignocellulosic materials," *Reviews in Environmental Science and Bio/Technology*, vol. 14, no. 2, pp. 211–228, 2015.

[9] V. S. Munagapati, J.-C. Wen, C.-L. Pan, Y. Gutha, and J.-H. Wen, "Enhanced adsorption performance of reactive red 120 azo dye from aqueous solution using quaternary amine modified orange peel powder," *Journal of Molecular Liquids*, vol. 285, pp. 375–385, 2019.

[10] R. M. Naik, "Use of orange peel as an adsorbent for the removal of Cr(VI) from its aqueous solution," *Indian Journal Chemical. Technology*, vol. 25, no. 3, pp. 300–305, 2018.

[11] C. Tejada-Tovar, A. Herrera-Barros, A. Villabona-Ortíz, Á. González-Delgado, and J. Núñez-Zarur, "Hexavalent chromium adsorption from aqueous solution using orange peel modified with calcium chloride: equilibrium and kinetics study," *Indian Journal of Science and Technology*, vol. 11, pp. 1–10, 2018.

[12] C. Hadj-Otmane, A. Ouakouak, F. Touahra, H. Grabi, J. Martín, and M. Bilal, "Date palm petiole-derived biochar: effect of pyrolysis temperature and adsorption properties of hazardous cationic dye from water," *Biomass Conversion and Biorefinery*, vol. 343, no. 6, pp. 1–11, 2022.

[13] A. Naima, F. Ammar, O. Abdelkader et al., "Development of a novel and efficient biochar produced from pepper stem for effective ibuprofen removal," *Bioresource Technology*, vol. 347, article 126685, 2022.

[14] M. T. Amin, A. A. Alazba, and M. Shafiq, "Application of the biochar derived from orange peel for effective biosorption of copper and cadmium in batch studies: isotherm models and kinetic studies," *Arabian Journal of Geosciences*, vol. 12, no. 2, pp. 1–12, 2019.

[15] J. P. Song, S. S. Zhang, G. X. Li, Q. Du, and F. Yang, "Preparation of montmorillonite modified biochar with various temperatures and their mechanism for Zn ion removal," *Journal of Hazardous Materials*, vol. 391, article 121692, 2020.

[16] Q. L. Wu, Y. Xian, Z. L. He et al., "Adsorption characteristics of Pb(II) using biochar derived from spent mushroom substrate," *Scientific Reports*, vol. 9, no. 1, pp. 1–11, 2019.

[17] H.-O. Chahinez, O. Abdelkader, Y. Leila, and H. N. Tran, "One-stage preparation of palm petiole-derived biochar: characterization and application for adsorption of crystal violet dye in water," *Environmental Technology and Innovation*, vol. 19, article 100872, 2020.

[18] H. Y. Guo, L. J. Ma, F. Shen et al., "Effects of La-involvement on biomass pyrolysis behaviors and properties of produced biochar," *Journal of Rare Earths*, vol. 35, no. 6, pp. 593–601, 2017.

[19] L. H. Nguyen, H. T. Van, Q. T. Nguyen et al., "Paper waste sludge derived-hydrochar modified by iron (III) chloride for effective removal of Cr(VI) from aqueous solution: kinetic and isotherm studies," *Journal of Water Process Engineering*, vol. 39, article 101877, 2021.

[20] M. Torab-Mostaedi, M. Asadollahzadeh, A. Hemmati, and A. Khosravi, "Biosorption of lanthanum and cerium from aqueous solutions by grapefruit peel: equilibrium, kinetic and thermodynamic studies," *Research on Chemical Intermediates*, vol. 41, no. 2, pp. 559–573, 2015.

[21] C. Tejada-Tovar, Á. González-Delgado, and Á. Villabona-Ortíz, "Adsorption kinetics of orange peel biosorbents for Cr(VI) uptake from water," *Contemporary Engineering Sciences*, vol. 11, no. 24, pp. 1185–1193, 2018.

[22] N. C. Feng and X. Y. Guo, "Characterization of adsorptive capacity and mechanisms on adsorption of copper, lead and zinc by modified orange peel," *Transactions of Nonferrous Metals Society of China*, vol. 22, no. 5, pp. 1224–1231, 2012.

[23] L. Liu, Y. Z. Rao, C. S. Tian et al., "Adsorption performance of La(III) and Y(III) on orange peel: impact of experimental variables, isotherms, and kinetics," *Adsorption Science and Technology*, vol. 2021, article 7189639, 12 pages, 2021.

[24] E. Vences-Alvarez, L. H. Velazquez-Jimenez, L. F. Chazaro-Ruiz, P. E. Diaz-Flores, and J. R. Rangel-Mendez, "Fluoride removal in water by a hybrid adsorbent lanthanum-carbon," *Journal of Colloid and Interface Science*, vol. 455, pp. 194–202, 2015.

[25] E. Kusrini, A. Usman, F. A. Sani, L. D. Wilson, and M. A. A. Abdullah, "Simultaneous adsorption of lanthanum and yttrium from aqueous solution by durian rind biosorbent," *Environmental Monitoring and Assessment*, vol. 191, no. 8, pp. 1–8, 2019.

[26] Y. N. Ji, N. Zheng, Q. R. An et al., "The effect of carbonization temperature on the capacity and mechanisms of Cd(II)-Pb(II) mix-ions adsorption by wood ear mushroom sticks derived biochar," *Environmental Monitoring and Assessment*, vol. 239, article 113646, 2022.

[27] Y. H. Zhong, C. L. Peng, G. S. Wang, L. Qin, and S. L. Hu, "Adsorption characteristics and mechanism of Y(III) by montmorillonite," *Journal of the Chinese Society of Rare Earths*, vol. 37, pp. 713–723, 2019.

[28] S. B. Yang, N. Okada, and M. Nagastu, "The highly effective removal of Cs+ by low turbidity chitosan-grafted magnetic bentonite," *Journal of Hazardous Materials*, vol. 301, pp. 8–16, 2016.

[29] Z. J. Yang, J. Hou, J. Wu, and L. Z. Miao, "The effect of carbonization temperature on the capacity and mechanisms of Pb(II) adsorption by microalgae residue-derived biochar," *Ecotoxicology and Environmental Safety*, vol. 225, article 112750, 2021.

[30] E. Allahkarami and B. Rezai, "Removal of cerium from different aqueous solutions using different adsorbents: a review," *Process Safety and Environmental Protection*, vol. 124, pp. 345–362, 2019.

[31] M. A. Jedrzejczyk, J. Engelhardt, M. R. Djokic et al., "Development of lignin-based mesoporous carbons for the adsorption of humic acid," *ACS Omega*, vol. 6, no. 23, pp. 15222–15235, 2021.

[32] M. A. Hubbe, S. Azizian, and S. Douven, "Implications of apparent pseudo-second-order adsorption kinetics onto cellulosic materials: a review," *BioResources*, vol. 14, no. 3, pp. 7582–7626, 2019.

[33] R. Nadeem, Q. Manzoor, M. Iqbal, and J. Nisar, "Biosorption of Pb(II) onto immobilized and native Mangifera indica waste biomass," *Journal of Industrial and Engineering Chemistry*, vol. 35, pp. 185–194, 2016.

[34] V. H. Nguyen, H. T. Van, V. Q. Nguyen, X. V. Dam, L. P. Hoang, and L. T. Ha, "Magnetic Fe_3O_4 nanoparticle biochar derived from pomelo peel for reactive red 21 adsorption from aqueous solution," *Journal of Chemistry*, vol. 2020, Article ID 3080612, 14 pages, 2020.

[35] Q. Shu, C. F. Liao, W. Q. Zou, B. Q. Xu, and Y. H. Tan, "Recovery of rare earth element ytterbium (III) by dried powdered biomass of spirulina: adsorption isotherm, kinetic and thermodynamic study," *Transactions of Nonferrous Metals Society of China*, vol. 31, no. 4, pp. 1127–1139, 2021.

[36] L. S. Ismail and F. I. Khalili, "Biosorption of neodymium(III) and cerium(III) ions by loquat leave (*Eriobotrya japonica*) kinetics and thermodynamic studies," *Desalination and Water Treatment*, vol. 229, pp. 291–301, 2021.

[37] S. Iftekhar, D. L. Ramasamy, V. Srivastava, M. B. Asif, and M. Sillanpää, "Understanding the factors affecting the adsorption of lanthanum using different adsorbents: a critical review," *Chemosphere*, vol. 204, pp. 413–430, 2018.

[38] G. Z. Kyzas, N. K. Lazaridis, and A. C. Mitropoulos, "Removal of dyes from aqueous solutions with untreated coffee residues as potential low-cost adsorbents: equilibrium, reuse and thermodynamic approach," *Chemical Engineering Journal*, vol. 189-190, pp. 148–159, 2012.

[39] Y. Y. Wang, H. H. Lu, Y. X. Liu, and S. M. Yang, "Ammonium citrate-modified biochar: an adsorbent for La(III) ions from aqueous solution," *Colloids and Surfaces: A*, vol. 509, pp. 550–563, 2016.

[40] D. Kołodyńska, J. Bąk, M. Majdańska, and D. Fila, "Sorption of lanthanide ions on biochar composites," *Journal of Rare Earths*, vol. 36, no. 11, pp. 1212–1220, 2018.

[41] D. Zhou, *Remediation of Contaminated Soil Using Biochar in Ion-Absorbed Rare Earth Ore Area*, Jiangxi University of Science and Technology, 2018.

[42] E. M. Iannicelli-Zubiani, P. G. Stampino, C. Cristiani, and G. Dotelli, "Enhanced lanthanum adsorption by amine modified activated carbon," *Chemical Engineering Journal*, vol. 341, pp. 75–82, 2018.

[43] Q. Cheng, "Study on the adsorption of lanthanum (III) from aqueous solution by bamboo charcoal," *Journal of Rare Earths*, vol. 28, pp. 125–131, 2010.

[44] E. Kusrini, M. I. Alhamid, A. B. Widiantoro, N. Z. A. Daud, and A. Usman, "Simultaneous adsorption of multi-lanthanides from aqueous silica sand solution using pectin-activated carbon composite," *Arabian Journal for Science and Engineering*, vol. 45, no. 9, pp. 7219–7230, 2020.

[45] E. Kusrini, D. D. Kinastiti, L. Wilson, A. Usman, and A. Rahman, "Adsorption of lanthanide ions from aqueous solution in multicomponent systems using activated carbon from banana peels (*Musa paradisiaca* L.)," *International Journal of Technology*, vol. 9, no. 6, p. 1132, 2018.

[46] D. Sadovsky, A. Brenner, B. Astrachan, B. Asaf, and R. Gonen, "Biosorption potential of cerium ions using spirulina biomass," *Journal of Rare Earths*, vol. 34, no. 6, pp. 644–652, 2016.

[47] L. P. Hoang, H. T. Van, T. T. H. Nguyen, V. Q. N. Nguyen, and P. Q. Thang, "Coconut shell activated carbon/$CoFe_2O_4$ composite for the removal of rhodamine B from aqueous solution," *Journal of Chemistry*, vol. 2020, Article ID 9187960, 12 pages, 2020.

[48] H. Wang, Q. Chen, R. Liu, Y. Zhang, and Y. Zhang, "Synthesis and application of starch-stablized Fe-Mn/biochar composites for the removal of lead from water and soil," *Chemosphere*, vol. 305, article 135494, 2022.